Journal of Asian Ceramic Societies 3 (2015) 345–351

HOSTED BY

Contents lists available at ScienceDirect

Journal of Asian Ceramic Societies

journal homepage: www.elsevier.com/locate/jascer

Synthesis, characterizations, antibacterial and photoluminescence studies of solution combustion-derived α-Al_2O_3 nanoparticles

P.A. Prashanth [a], R.S. Raveendra [a,b,*], R. Hari Krishna [c], S. Ananda [d], N.P. Bhagya [a], B.M. Nagabhushana [c], K. Lingaraju [e], H. Raja Naika [e]

[a] R & D Center, Department of Chemistry, Sai Vidya Institute of Technology, Bengaluru 560 064, India
[b] Research and Development Centre, Bharathiar University, Coimbatore, Tamilnadu 641 046, India
[c] Department of Chemistry, M.S. Ramaiah Institute of Technology, Bengaluru 560054, India
[d] Department of Chemistry, University of Mysore, Manasa Gangotri, Mysore 570 006, India
[e] Department of Studies and Research in Environmental Science, Tumkur University, Tumkur 572 103, India

ARTICLE INFO

Article history:
Received 23 March 2015
Received in revised form 4 July 2015
Accepted 4 July 2015
Available online 29 July 2015

Keywords:
α-Al_2O_3
Solution combustion synthesis
Antibacterial
Staphylococcus aureus
Photoluminescence

ABSTRACT

In this work, we report a novel, economical, low temperature solution combustion synthesis (SCS) method to prepare α-Al_2O_3 (Corundum) nanoparticles. Powder X-ray diffraction (PXRD), field emission scanning electron microscopy (FE-SEM), high-resolution transmission electron microscopy (HR-TEM), Fourier transform infrared spectroscopy (FT-IR), BET surface area and ultraviolet visible spectroscopy (UV–vis) measurements were used to characterize the product. Antibacterial studies were examined against gram −ve *Klebsiella aerogenes, Escherichia coli, Pseudomonas desmolyticum* and gram +ve *Staphylococcus aureus* bacteria by agar well diffusion method. The α-Al_2O_3 nanoparticles showed substantial effect on all the four bacterial strains. Photoluminescence (PL) measurements under excitation at about 255 nm show that the alumina nanoparticles have emission peaks at 394 and 392 nm.

© 2015 The Ceramic Society of Japan and the Korean Ceramic Society. Production and hosting by Elsevier B.V. All rights reserved.

1. Introduction

Discoveries in the past decade have shown that once materials are prepared in the form of very small particles, they change significantly. Their physical and chemical properties sometimes change to the extent that completely new phenomena are established. The rising demand for inorganic phosphor materials in different applications, such as white LEDs, fluorescent lamps, long-lasting phosphors, X-ray imaging, high-definition television screens, field-emission displays, luminous paints, electroluminescent devices and ceramics products, has concerned researchers to discover new materials [1,2].

Over the past few years, extensive research work is dedicated to the field of Nanotechnology and Nanoscience. The current worldwide nanotechnology revolution is predicted to impact several areas of biomedical research and other science and engineering applications. Nanoparticles-assisted drug delivery, cell imaging and cancer therapy are important applications of nanotechnology [3]. Other important application of nanoparticles is its enhanced antibacterial activity compared to its bulk counterparts. With increasing concerns of bacterial infections, there is a growing need to develop new and powerful antibacterial agents. In this direction, already nanoparticles have been applied in food preservation [4], burn dressings [5], safe cosmetics [6], medical devices [7], water treatment [8] and other range of products [9–13], due to its excellent antibacterial activity on several gram positive and negative bacteria [14]. There are various parameters that can affect the bactericidal property of the nanoparticles, namely size, shape, morphology, stability and surface functionalization. In the past few years, there is lot of interest on inorganic nanoparticles as antibacterial agents due to their improved stability and ecofriendly nature compared with the classical organic antibacterial agents [15]. There are several classes of inorganic nanoparticles such as nanometals [12], metal salts [16] metal oxides [17], metal hydroxides [18] and hybrid materials [19] that show antibacterial activity. Among the listed novel antibacterial agents, metal oxides are more extensively studied for their ease of synthesis and higher stability. Hence, there is great need for the research and development of newer oxide-based antibacterial agents. One of the potential oxide-based stable antibacterial nanoparticles studied is Al_2O_3. The α-Al_2O_3 nanoparticles showed a significant toxicity towards a dominant microbial

* Corresponding author at: R & D Center, Department of Chemistry, Sai Vidya Institute of Technology, Bengaluru 560 064, India. Tel.: +91 9880796678.
E-mail address: raveendrars@gmail.com (R.S. Raveendra).
Peer review under responsibility of The Ceramic Society of Japan and the Korean Ceramic Society.

http://dx.doi.org/10.1016/j.jascer.2015.07.001
2187-0764 © 2015 The Ceramic Society of Japan and the Korean Ceramic Society. Production and hosting by Elsevier B.V. All rights reserved.

species (*Bacillus licheniformis*) at a low concentration (1 μg/mL) [20]. It is reported by various authors that there are several methods available to prepare α-Al_2O_3 nanoparticles. Sharma et al. have prepared α-Al_2O_3 nanoparticles at lower temperature and demonstrated the effectiveness of seeding by aluminium hydroxide in directing the crystallization of the desired α-Al_2O_3 phase [21]. Tok et al. have reported on inexpensive flame spray pyrolysis method to prepare agglomerated, free, nano-sized Al_2O_3 nanoparticles with a size range of 5–30 nm [22]. α-Al_2O_3 nanowires and nanobelts have been successfully synthesized from Al pieces and SiO_2 nanoparticles at 1200 °C and 1150 °C, respectively in Ar atmosphere by Peng et al. [23]. Naskar has synthesized the alumina nanoparticles from hydrothermal process at 170 °C for 6 h using glucose and other water-based precursor materials [24]. Khamirul Amin Matori et al. have reported on a recycling project in which α-Al_2O_3 was produced from aluminium cans with sulphuric acid at 1200 °C [25]. Sourav Ghose et al. have studied the role of tetramethyl urea on the formation of mesoporous alumina from hydrothermal method at 150 °C for 6–24 h [26].

In the present study, we are presenting synthesis of α-Al_2O_3 nanoparticles by facile low temperature solution combustion method, characterized by different techniques to substantiate the product and investigated their antibacterial activity towards gram −ve *Klebsiella aerogenes, Escherichia coli, Pseudomonas desmolyticum* and gram +ve *Staphylococcus aureus* bacteria by agar well diffusion method. Photoluminescence spectra were recorded in order to study its optical behaviour.

2. Experimental

2.1. Materials and methods

All the chemicals and reagents used in this study were of analytical grade. Commercially pure aluminium nitrate ($Al(NO_3)_3{\cdot}9H_2O$, 99% Merck), urea ($CO(NH_2)_2$ 99% Merck), nutrient agar media, Ciprofloxacin (Hi Media, Mumbai, India), and double-distilled water.

2.2. Synthesis of α-Al_2O_3 nanoparticles

To synthesize α-Al_2O_3 nanoparticles solution combustion synthesis method was used [27,28]. Fuel type and fuel/aluminium nitrate molar ratio proved to be of great importance during the preparation of α-Al_2O_3 powders [29,30]. The stoichiometry of the redox mixture for combustion is calculated based on the total oxidizing and reducing valencies of the oxidizer and the fuel using the concept of propellant chemistry. The amounts of metal nitrates to fuel ratios for the synthesis of the nanoparticles are based on the following equation.

$$\text{Oxidizer/fuel ratio} = \frac{\sum \text{Valencies of all oxidizing and reducing elements in oxidizer}}{(-1)\sum \text{Valencies of all oxidizing ad reducing elements in fuel}} \quad (1)$$

$Al(NO_3)_3{\cdot}9H_2O$ and $CO(NH_2)_2$ were used as oxidizer and fuel, respectively, precursor mixture was magnetically stirred well in a crystalline dish for about 30 min with distilled water to get homogeneous mixture, and then it was introduced into the pre-heated muffle furnace at 500 ± 10 °C. The solution was boiled and the resulted viscous liquid catches fire, auto ignited with flames on the surface, which rapidly proceeded throughout the entire volume forming a white powdered product. The overall reaction can be written as

$$2Al(NO_3)_3 + 3CO(NH_2)_2 \rightarrow Al_2O_3 + 6H_2O + 6N_2 + 3CO_2 \quad (2)$$

2.3. Characterization techniques

To find out the phase formation, α-Al_2O_3 nanoparticles were characterized by PXRD. Powder X-ray diffraction patterns were recorded on a Shimadzu XRD-700 X-ray Diffractometer with CuKα radiation with diffraction angle range $2\theta = 20^\circ$ to 80° operating at 40 kV and 30 mA. To study the crystallite size and morphology of the product, HR-TEM analysis was performed on a Hitachi H-8100 (accelerating voltage up to 200 kV, LaB6 Filament). FE-SEM was performed on a ZEISS ULTRA 55 scanning electron microscope. The FT-IR studies have been recorded on a Perkin–Elmer Spectrometer (Spectrum 1000) with KBr pellet method in the range of 400–4000 cm^{-1}. The total surface area of the synthesized alumina nanoparticles was measured using nitrogen adsorption/desorption isotherms with a Brunauer–Emmett–Teller (BET) surface area analyzer (ASAP 2020) at the bath temperature −196.329 °C. To calculate optical energy band gap UV–vis spectrum was recorded using ElicoSL-210 UV–vis spectrophotometer. Photoluminescence excitation and emission spectra were recorded using Perkin–Elmer LS-55 luminescence spectrophotometer equipped with Xe lamp.

2.4. Antibacterial studies

The pathogenic bacterial strains used in this study are gram −ve bacteria, namely *K. aerogenes* [NCIM-2098], *E. coli* [NCIM-5051], *P. desmolyticum* [NCIM-2028] and gram +ve bacteria, *S. aureus* [NCIM-5022]. The agar well diffusion method was used for the assessment of antibacterial activity of α-Al_2O_3. Nutrient Media was poured into sterilized Petri dishes. LB broth was seeded with 24 h incubated cultures of the respective clinical isolates and the individual bacterial strains were spread separately on the agar medium. The well is made by using sterile cork borer and wells of 6 mm diameter are created into each petri-plate under aseptic conditions. Various concentrations of nanoparticles (i.e. 500 mg, 1000 mg/well) are used to assess the activity of the nanoparticle. The nanoparticles are dispersed in sterile water and are added into the wells by using sterile micropipettes. Simultaneously, the standard antibiotic Ciprofloxacin (as positive control), is tested against the pathogens. Plates were then incubated at 37 °C for 36 h. After the incubation period, the zone of inhibition of each well was measured and the values were noted. Triplicates were maintained in each compound and the average values were calculated in millimetre (mm) for the ultimate antibacterial activity.

2.5. Photoluminescence studies

Photoluminescence excitation and emission spectra of α-Al_2O_3 was recorded by taking sample of known weight in the solid sample holder of Perkin–Elmer LS-55 luminescence spectrophotometer equipped with Xe lamp. From the excitation spectra, prominent excitation wavelengths are selected and the emission spectrum was recorded for the selected excitation wavelengths.

3. Result and discussions

3.1. PXRD studies for phase formation and crystallite size

Previous studies reported that the formation of the crystalline phase of α-Al_2O_3 passes by means of thermal treatment through the following series of polymorphic phase transformation before final conversion to the thermodynamically stable phase α-Al_2O_3 polymorph (Corundum) [31].

$$\text{Precursor} \rightarrow \gamma \rightarrow \delta \rightarrow \theta \rightarrow \alpha\text{-Alumina} \quad (3)$$

The mechanism for the α-Al_2O_3 phase transformation through precursor has been postulated and discussed previously and

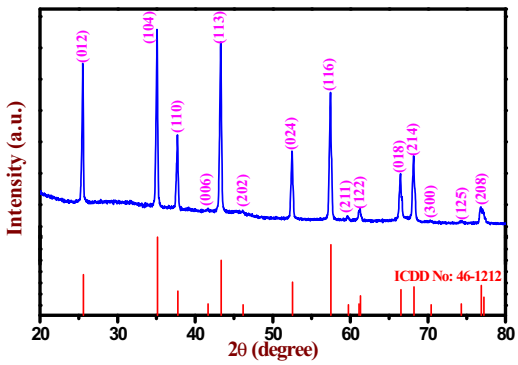

Fig. 1. PXRD patterns of α-Al_2O_3 nanoparticles.

confirmed that α-Al_2O_3 was formed through the nucleation and growth process [32]. As θ-Al_2O_3 phase transformation proceeds, α-Al_2O_3 nuclei appear at certain sites in the matrix of θ-Al_2O_3 crystallites firstly. And this is subsequently followed by the growth of the nuclei into the surrounding matrix. During the growth stage, the interface between the α-Al_2O_3 nuclei and parent matrix migrates into the θ-Al_2O_3 matrix [33] and the mechanism of "interface controlled" is proposed [34].

The formation of nanocrystalline phase of the combustion-derived product was confirmed by PXRD measurements. The PXRD results were examined with Crystallographica Search-Match (CSM). The PXRD of sample shows the crystalline nature of sample having rhombohedral structure (matched with ICDD card number 46-1212 with space group R-3c (No-167)), and cell parameters $a = 4.7587$ Å, $b = 4.7587$ Å and $c = 12.9929$ Å. All the diffraction peaks can be indexed to (0 1 2), (1 0 4), (1 1 0), (0 0 6) (1 1 3), (2 0 2), (0 2 4), (1 1 6), (2 1 1), (1 2 2), (0 1 8), (2 1 4), (3 0 0), (1 2 5) and (2 0 8) reflections. The broadening of the reflections clearly indicates the inherent nature of nanocrystals. Fig. 1 shows the powder X-ray diffraction pattern of α-Al_2O_3 nanoparticles. The crystallite size is calculated from the full width at half maximum (FWHM (β)) of the diffraction peaks using Debye–Scherer's method [35] using the following equation:

$$d = \frac{k\lambda}{\beta \cos\theta} \tag{4}$$

where 'd' is the average crystalline dimension perpendicular to the reflecting phases, 'λ' is the X-ray wavelength, 'k' is Scherer's constant (0.92), 'β' is the full width at half maximum (FWHM) intensity of a Bragg reflection excluding instrumental broadening and 'θ' is the Bragg's angle. The calculated average crystallite size of the product is found in the range of 20–30 nm. Crystallite size was also calculated from Williamson and Hall (W–H) plots [36] by the following equation:

$$\beta \cos\theta = \varepsilon(4 \sin\theta) + \frac{\lambda}{D} \tag{5}$$

where 'β' (FWHM in radian) is measured for different XRD lines corresponding to different planes. 'θ' is the Bragg's angle, 'ε' is the strain developed, 'λ' is the X-ray wavelength and 'D' is the grain size. The average crystallite size is found to be 18 nm. Fig. 2 shows the W–H plot of the α-Al_2O_3 nanoparticles. The crystal structure of the α-Al_2O_3 nanoparticles was evaluated using DIAMOND-crystal and

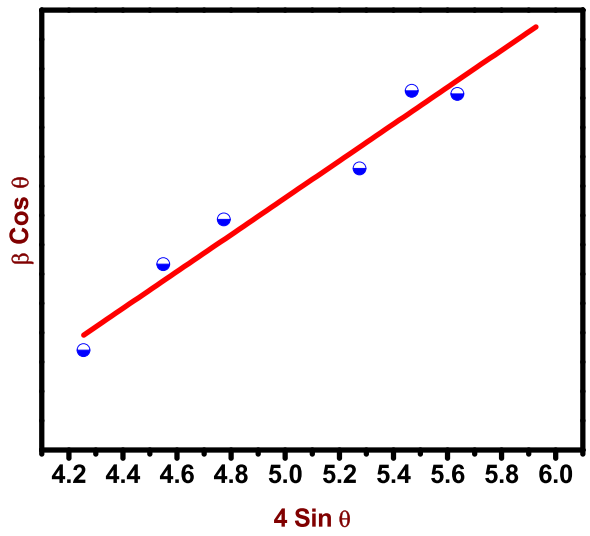

Fig. 2. W–H plot of α-Al_2O_3 nanoparticles.

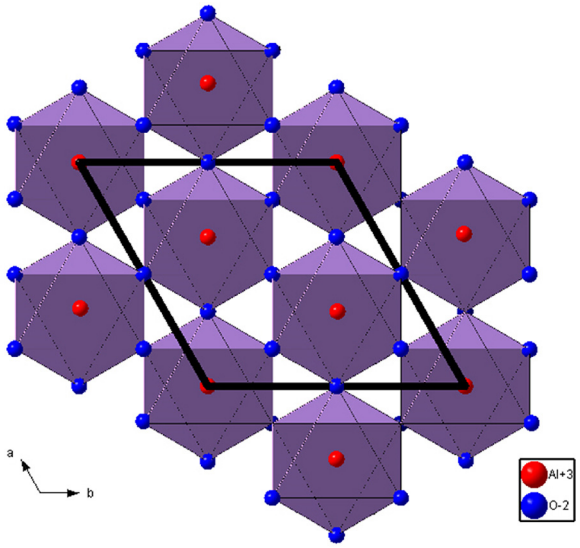

Fig. 3. Packing diagram of α-Al_2O_3 nanoparticles.

molecular structure visualization software with the help of PXRD data. Lattice and the structural parameters of the α-Al_2O_3 nanoparticles are summarized in Table 1. Fig. 3 shows the packing diagram of α-Al_2O_3 nanoparticles.

3.2. FT-IR spectroscopic studies

Fig. 4 represents FT-IR spectrum of the product recorded to define the vibrational frequency of Metal–Oxygen and other bonds related to impurities present in the α-Al_2O_3 nanoparticles. It can be seen that no impurity peaks corresponding to the organic matter were observed. However, a weak band can be seen at 2350 cm^{-1} which is attributed to the stretching vibration of the C—H bond of

Table 1
Crystal lattice and structural parameters of α-Al_2O_3 nanoparticles.

Atoms	Oxidation state	Wyckoff notation	*x*	*y*	*z*	Occupancy
Al	3+	6a	0.0000	0.0000	0.2500	1
O	2−	18b	0.5000	0.0000	0.0000	1

Crystal system: Rhombohedral; space group: R-3c (167); point group: 3-m1, hexagonal axis; cell volume = 254.98 (Å)^3.

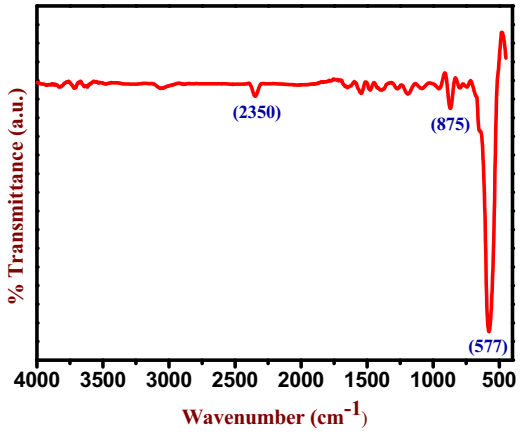

Fig. 4. FTIR spectrum of α-Al_2O_3 nanoparticles.

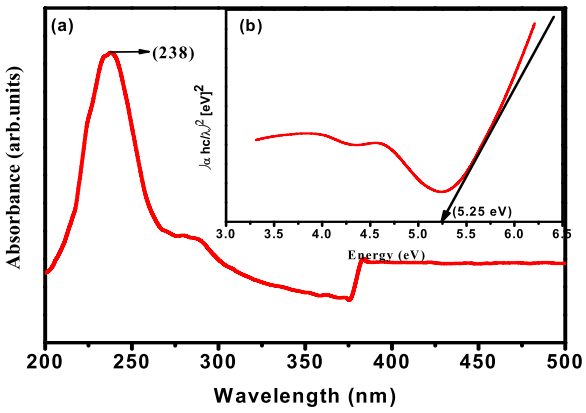

Fig. 5. (a) UV–vis spectrum of α-Al_2O_3 nanoparticles; (b) optical energy band gap.

methyl group in urea. Strong absorption bands at 577 cm^{-1} can be assigned to the stretching vibration of Al—O bond.

3.3. UV–visible spectroscopic studies and evaluation of the band gap energy

In order to determine the optical energy band gap of sample, the UV–vis absorption spectrum was recorded. The sample shows a strong absorption peak (λ_{max}) at 238 nm in the UV region. Fig. 5a shows the UV–vis absorption spectrum of sample. This can be attributed to photoexcitation of electron from valence band to conduction band. The optical energy band gap (E_g) was estimated (Fig. 5b) by the method proposed by Wood and Tauc [37] according to the following equation;

$$(h\nu\alpha) \propto (h\nu - E_g)^n \quad (6)$$

where 'α' is the absorbance, 'h' is the Planck's constant, 'ν' is the frequency, 'E_g' is the optical energy band gap and 'n' is a constant associated to the different types of electronic transitions (n = 1/2, 2, 3/2 or 3 for direct allowed, indirect allowed, direct forbidden and indirect forbidden transitions, respectively). E_g value for α-Al_2O_3 nanoparticles is ~5.25 eV.

3.4. Morphological analysis

The morphology of synthesized α-Al_2O_3 nanoparticles obtained from the solution combustion method was investigated using field emission scanning electron microscopy Fig. 6(a–c) shows FE-SEM images of α-Al_2O_3 nanoparticles. It revealed that the morphology of the α-Al_2O_3 nanoparticles was a nonspherical shape, i.e. flakes-like and has uniform size and distribution. The proof for the crystallinity of the nanoparticles was obtained by TEM investigations. The TEM method is better than X-ray line broadening; in that, it is direct and less likely to be affected by experimental errors and/or other properties of the particles such as internal strain or distribution in the size of the lattice parameter. TEM and HR-TEM images of α-Al_2O_3 nanoparticles (Fig. 7 (a–c)) show that the particles obtained are in nano regime and highly crystalline, and have average particle size of ~20 nm. Further, HRTEM figures clearly show that the fringes are oriented in different directions (marked with circles) corresponding to the different planes. This also shows the polycrystalline nature of the sample.

3.5. BET surface area measurement

The total surface areas of the samples were obtained with reference to the Brunauer–Emmett–Teller (BET) multi-point and single-point methods [38] using the N_2 adsorption/desorption isotherm data. Before analysis, all of the obtained alumina nanoparticles were evacuated under vacuum condition at 150 °C overnight in order to clean all the pores. The pore volume data were calculated by using BJH method, which is the procedure for calculating pore size distribution using the Kelvin equation and DH methods. The micropore volumes of the samples were obtained using Dubinin–Radushkevich (DR) method [39]. The pore size distribution was determined by using the BJH model. All experimental parameters of BET surface area analysis are summarized in Table 2. Fig. 8 (a and b) shows the N_2 adsorption/desorption isotherms and BET surface area plot of alumina nanoparticles.

3.6. Antibacterial studies

Antibacterial activity of alumina nanoparticles has already been investigated by various authors [40–42]. However, combustion-derived products retain their interesting properties till today due to their unique characteristics. The detailed procedure followed for antibacterial studies is described in Section 2.4. The antibacterial property of α-Al_2O_3 nanoparticles was evaluated against gram −ve *K. aerogenes, E. coli, P. desmolyticum* and gram +ve *S. aureus*

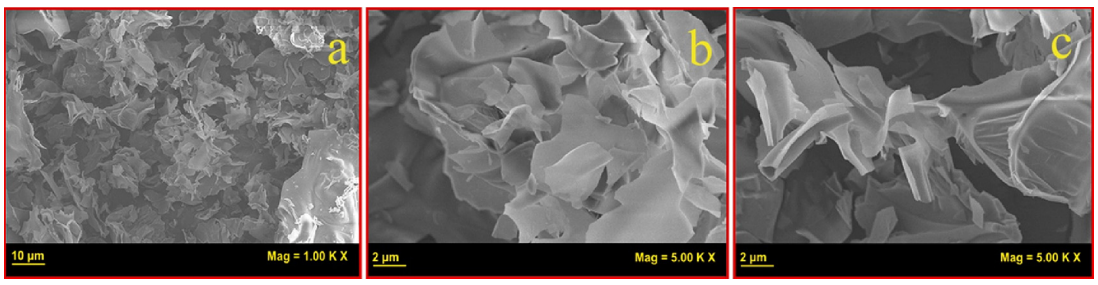

Fig. 6. (a–c) FE-SEM micrographs of α-Al_2O_3 nanoparticles.

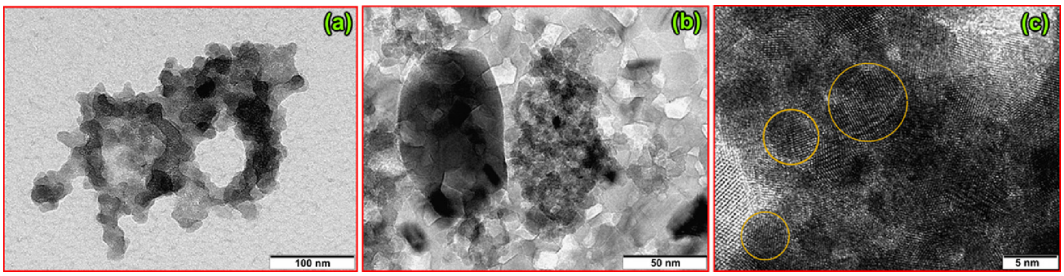

Fig. 7. (a and c) TEM; (b) HR-TEM of α-Al_2O_3 nanoparticles.

Table 2
BET surface area parameters.

Surface area	Pore volume (cm^3/g)	Pore size (nm)	Micropore s. area (m^2/g)	BJH adsorption average pore diameter (nm)	BJH desorption average pore diameter (nm)
36.00 (m^2/g)	0.01	1.30	40.10	107.00	1.30

Table 3
Antibacterial activity of α-Al_2O_3 nanoparticles on pathogenic bacterial strains.

Sl. no	Treatment	*Klebsiella aerogenes* (Mean ± SE)	*Escherichia coli* (Mean ± SE)	*Pseudomonas desmolyticum* (Mean ± SE)	*Staphyloccus aureus* (Mean ± SE)
I	Standard (5 mg/50 mL)	10.00 ± 0.00	11.70 ± 0.33**	9.70 ± 0.33**	10.70 ± 0.33**
II	α-Al_2O_3 (500 mg/50 mL)	1.30 ± 0.33**	1.00 ± 0.00	1.00 ± 0.00	1.70 ± 0.33**
III	α-Al_2O_3 (1000 mg/150 mL)	2.70 ± 0.33*	2.33 ± 0.33**	2.70 ± 0.33**	3.70 ± 0.00

Values are the mean ± SE of inhibition zone in mm.
Asterisks symbols represent statistical significance, $^*P < 0.05$, $^{**}P < 0.01$ as compared with the control group.

bacteria using agar well diffusion method. The results show that the negative control, DMSO (labelled as C in Fig. 9), did not show any inhibition zone, which means that the control alone without nanoparticles does not show any antibacterial activity. When the loading of nanoparticles (α-Al_2O_3) was 500 mg, among the gram negative bacteria investigated, the inhibition of *K. aerogenes* is better than the other two negative bacteria. However, when the load of nanoparticles was increased to 1000 mg, no significant difference in the inhibition zone was observed among the negative bacteria. The nanoparticles showed highest inhibition activity on the only positive bacteria studied, *S. aureus*. The zone of inhibition observed for this bacterial strain was 3.7 mm, which is higher than all the bacteria studied for the same loading of nanoparticles. Further, the statistical error was evaluated using ezAnova statistical software and the *P* value was found to be <0.05 indicating that the error is well within the limit. The zone of inhibition is given in Fig. 9 (a–d) and data are given in Table 3.

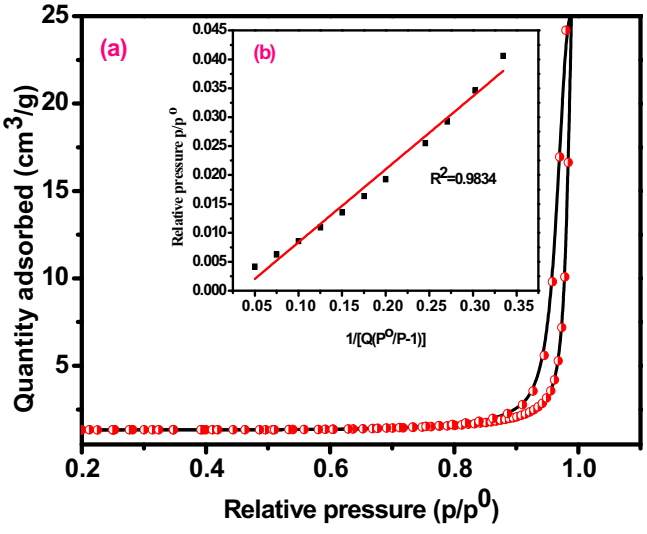

Fig. 8. (a and b) BET surface area.

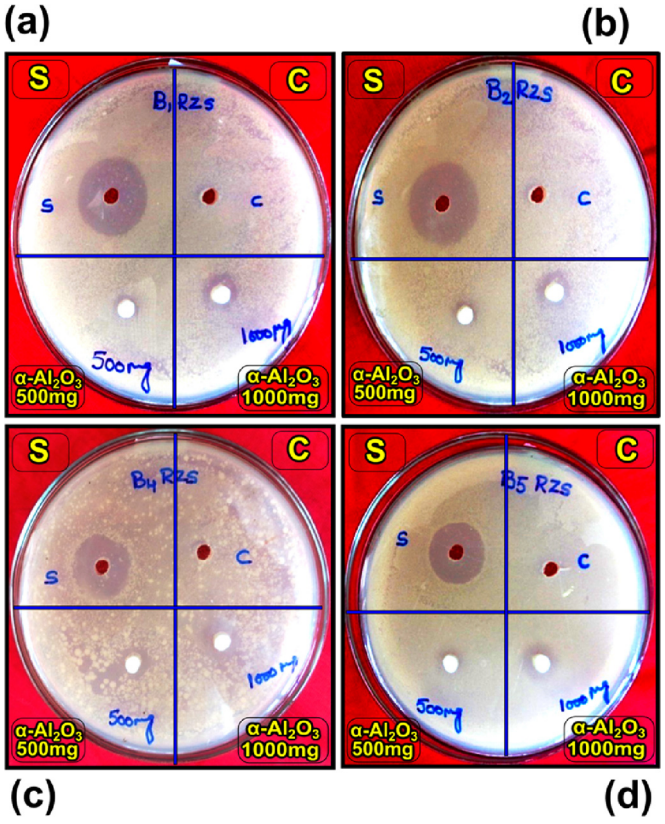

Fig. 9. Zone of inhibition tests for α-Al_2O_3 nanoparticles against: (a) *K. aerogenes*; (b) *E. coli*; (c) *P. desmolyticum*; (d) *S. aureus*.

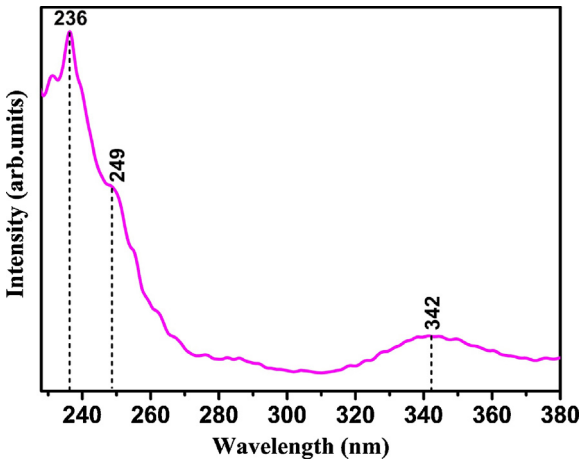

Fig. 10. PL excitation spectrum of α-Al_2O_3 nanoparticles.

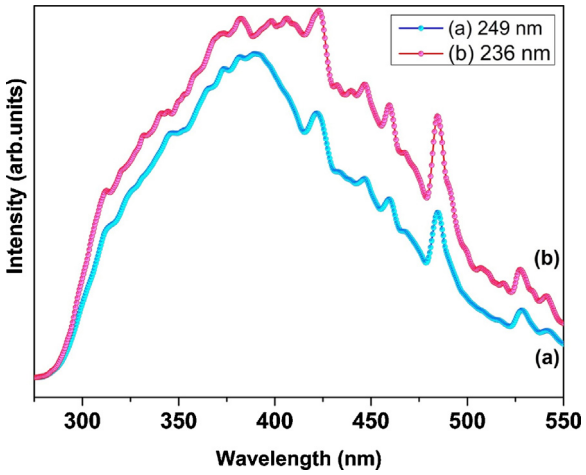

Fig. 11. PL emission spectrum of α-Al_2O_3 nanoparticles excited at (a) 249 nm and (b) 236 nm.

3.7. Mechanism of antibacterial activity

The following factor may be responsible for the antibacterial activity, viz. (i) the cationic size of α-Al_2O_3 nanoparticles and (ii) reactive oxygen species (ROS) formation [43]. The antibacterial effect of these α-Al_2O_3 nanoparticles seems to be administered by the presence of ionic and colossal structural patterns, which is in good agreement with the pharmacophore. The presence of these helps the compounds to interact or penetrate more with cell membrane of the bacteria, thereby inactivating them. This may be due to the distance between the positively charged groups and the nanoparticles. Another widely postulated mechanism is that of the "*self-promoted uptake*" [44] of the antibiotic across the outer membranes of bacteria, which consists of lipopolysaccharide surface. This suggests that the nanoparticles interact with the charged outer membrane and subsequent channel formation in the cytoplasmic membrane [45,46] resulting in cell death.

3.8. Photoluminescence (PL) studies

The photoluminescence (PL) excitation spectrum of as-formed α-Al_2O_3 is shown in Fig. 10. It shows three excitation bands centred at 236, 249 and 342 nm. It is interesting to note that the first band is sharp and the second and third bands are broad. The first and second bands at 236 and 249 nm are very commonly reported in undoped oxide samples that are ascribed to defects related to oxygen vacancies [47,48]. Further, the third band, due to its broadness and its peak position (342 nm), can be attributed to the carbon content in the samples [49,50]. Amorphous carbon present in the samples is due to the little carbonaceous matter from the fuel that remains. Speculation of amorphous carbon in the samples is very reasonable, as most of the literature reporting solution combustion technique support the claim of carbon impurities in the samples. Fig. 11 shows the photoluminescence spectrum of α-Al_2O_3 prepared using urea. Upon 236 nm excitation, a series of emission bands ranging from UV to green region are observed, and the bands were centred at 390, 421, 484 and 528 nm. Since Al^{3+} itself is non-luminous and the observed luminescence from α-Al_2O_3 samples must be due to non-stoichiometry created by the oxygen deficiency in the system, which is expected to arise when α-Al_2O_3 forms in carbon rich ambient [51]. A report by Shifa Wang et al. [52] showed that α-Al_2O_3-C composite exhibits luminescence due to carbon present in the samples and they have demonstrated that increase in the C content improved the luminescence property. Hence in our case, we believe that carbon related impurities typically from the fuel used in the synthesis technique significantly contribute for the observed luminescence of α-Al_2O_3.

In the emission spectra, the broad emission peak at 390 nm in UV region is attributed to radiative recombination of photo-generated hole with an electron occupying the oxygen vacancy [53]. Emission band centred at 421 nm is attributed to recombination of a delocalized electron close to the conduction band with a single charged state of surface oxygen vacancy [54]. The emission band at 484 nm can be attributed to self-trapped excitation luminescence [55]. Further, it should be noted that, except the peak intensities, there is no change in the emission spectrum observed with change in the excitation wavelength (Fig. 11).

4. Conclusions

The α-Al_2O_3 nanoparticles were successfully synthesized by simple SCS method and their characteristics were studied. Antibacterial activities were evaluated with four different bacterial pathogens. Results of antibacterial tests conclude that at higher concentrations (500 and 1000 μg), α-Al_2O_3 nanoparticles can act as a good antibacterial agent against of gram −ve *K. aerogenes, E. coli, P. desmolyticum* and gram +ve *S. aureus* bacteria in agar well diffusion method. Photoluminescence spectrum shows emission due to different kinds of defects. The PL emission in this particular study is ascribed to the presence of amorphous carbon and it is independent of the excitation wavelength.

Acknowledgements

The authors P.A. Prashanth and R.S. Raveendra thank the principal and management of Sai Vidya Institute of Technology, Bengaluru for their constant encouragement. Author R.S. Raveendra thanks Mr. Nagabhushana Patel of IISc, Bengaluru for his valuable help.

References

[1] P.K. Stoimenov, R.L. Klinger, G.L. Marchin and K.J. Klabunde, Langmuir, 18, 6679–6686 (2002).
[2] A. Suresh Kumar, R. Arun Kumar, R. Balasundaraprabhu, K. Senthil, S. Ramesh Kumar and V. Gunasekaran, Spectrochim. Acta A, 134, 283–287 (2015).
[3] M. Premanathan, K. Karthikeyan, K. Jeyasubramanian and G. Manivannan, Nanomed. Nanotech. Biol. Med., 7, 184–192 (2011).
[4] P. Prombutara, Y. Kulwatthanasal, N. Supaka, I. Sramala and S. Chareonpornwattana, Food Control, 24, 184–190 (2012).
[5] Y. Liu and H.-I. Kim, Carbohyd. Polym., 89, 111–116 (2012).

[6] S. Kokura, O. Handa, T. Takagu, T. Ishikawa, Y. Naito and T. Yoshikawa, Nanomed. Nanotechnol., 6, 570–574 (2010).
[7] L. Zhao, H. Wang, K. Huo, L. Cui, W. Zhang, H. Ni, Y. Zhang, Z. Wu and P.K. Chu, Biomaterials, 32, 5706–5716 (2011).
[8] H.R. Pant, D.R. Pandeya, K.T. Nam, W.-I. Baek, S.T. Hong and H.Y. Kim, J. Hazard. Mater., 189, 465–471 (2011).
[9] D. Martins, F.T.M. Costa, M. Brocchi and N. Duran, J. Nanopart. Res., 13, 355–363 (2011).
[10] B.A. Sevinc and L. Hanley, J. Biomed. Mater. Res. B, 94B, 22–31 (2010).
[11] M. Montazer, A. Shamei and F. Alimohammadi, Prog. Org. Coat., 74, 270–276 (2012).
[12] R. Kaegi, B. Sinnet, S. Zuleeg, H. Hagendorfer, E. Mueller, R. Vonbank, M. Boller and M. Burkhardt, Environ. Pollut., 158, 2900–2905 (2010).
[13] R. Prucek, J. Tucek, M. Kilianova, A. Panacek, L. Kvitek, J. Filip, M. Kolar, K. Tomankova and R. Zboril, Biomaterials, 32, 4704–4713 (2011).
[14] W.R. Li, X.B. Xie, Q.S. Shi, S.S. Duan, Y.S. Ouyang and Y.B. Chen, Biometals, 24, 135–214 (2011).
[15] R.K. Dutta, B.P. Nenavathu, M.K. Gangishetty and A.V.R. Reddy, Colloid. Surf. B, 94, 143–150 (2012).
[16] R. Chen, G. Cheng, M.H. So, J. Wu, Z. Lu, C.-M. Che and H. Sun, Mater. Res. Bull., 45, 654–658 (2010).
[17] S. Jadhav, S. Gaikwad, M. Nimse and A. Rajbhoj, J. Clust. Sci., 22, 121–129 (2011).
[18] C. Dong, J. Cairney, Q. Sun, O.L. Maddan, G. He and Y. Deng, J. Nanopart. Res., 12, 2101–2109 (2010).
[19] A.R. Abbasi, K. Akhbari and A. Morsali, Ultrason. Sonochem., 19, 846–852 (2012).
[20] S. Pakrashi, S. Dalai, D. Sabat, S. Singh, N. Chandrasekaran and A. Mukherjee, Chem. Res. Toxicol., 24, 1899–1904 (2011).
[21] P.K. Sharma, M.H. Jilavi, D. Burgard, R. Nass and H. Schmidt, J. Am. Ceram. Soc., 81, 2732–2734 (1998).
[22] A.I.Y. Tok, F.Y.C. Boey and X.L. Zhao, J. Mater. Process. Technol., 178, 270–273 (2006).
[23] X.S. Peng, L.D. Zhang, G.W. Meng, X.F. Wang, Y.W. Wang, C.Z. Wang and G.S. Wu, J. Phys. Chem. B., 106, 11163–11167 (2002).
[24] M.K. Naskar, J. Am. Ceram. Soc., 93, 1260–1263 (2010).
[25] K.A. Matori, L.C. Wah, M. Hashim, I. Ismail and M.H.M. Zaid, Int. J. Mol. Sci., 13, 16812–16821 (2012).
[26] S. Ghose, R. Dalapati and M.K. Naskar, J. Asian Ceram. Soc., 2, 380–386 (2014).
[27] T. Mimani and K.C. Patil, Mater. Phys. Mech., 4, 134–137 (2001).
[28] R.S. Raveendra, P.A. Prashanth, R. Hari Krishna, N.P. Bhagya, B.M. Nagabhushana, H. Raja Naika, K. Lingaraju, H. Nagabhushana and B. Daruka Prasad, J. Asian Ceram. Soc., 2, 357–365 (2014).
[29] R. Ianos, I. Lazau and C. Pacurariu, J. Mater. Sci., 44, 1016–1023 (2009).
[30] G. Ramesh, R.V. Mangalaraja, S. Anantha kumar and P. Manohar, Int. J. Phys. Sci., 8, 1729–1737 (2013).
[31] H.-L. Wen, Y.-Y. Chen, F-.S. Yen and C.-Y. Huang, Nanostruct. Mater., 11, 89–101 (1999).
[32] F.W. Dynys and J.W. Halloran, J. Am. Ceram. Soc., 65, 442–448 (1982).
[33] T.C. Chou and T.G. Nieh, J. Am. Ceram. Soc., 74, 2270–2279 (1991).
[34] H.-L. Wen and F.-S. Yen, J. Cryst. Growth, 208, 696–708 (2000).
[35] P. Klug and L.E. Alexander, X-ray Diffraction Procedure, Wiley, New York (1954).
[36] G.K. Williamson and W.H. Hall, Acta Metall., 1, 22–31 (1953).
[37] in Optical Properties of SolidsJ. Tauc and F. Abeles, North-Holland, Amsterdam (1970).
[38] S. Brunauer, P.H. Emmett and J. Teller, Am. Chem. Soc., 60, 309–319 (1938).
[39] M.M. Dubinin and L.V. Radushkevich, Proc. Acad. Sci. U.S.S.R: Phys. Chem. Sect., 55, 331–333 (1947).
[40] R. Gokulakrishnan, S. Ravikumar and J.A. Raj, Asian Pac. J. Trop. Dis., 2, 411–413 (2012).
[41] G. Geoprincy, N.N. Gandhi and S. Renganathan, Int. J. Pharm. Pharm. Sci., 4, 544–548 (2012).
[42] A. Mukherjee, I. Mohammed Sadiq, T.C. Prathna and N. Chandrasekaran, Sci. Micro Path Commu. Curr. Res. Technol. Adv., 1 Formatex, Microbiol. Ser., 3, 245–251 (2011).
[43] H.-U. Simon, A. Haj-Yehia and F. Levi-Schaffer, Apoptosis, 5, 415–418 (2000).
[44] R.M. Yeaman and N.Y. Yount, Pharmacol. Rev., 55, 27–55 (2003).
[45] D. Wu, Z. Chen, K. Cai, D. Zhuo, J. Chen and B. Jiang, Curr. Appl. Phys., 14, 1470–1475 (2014).
[46] K.R. Raghupathi, R.T. Koodali and A.C. Manna, Langmuir, 27, 4020–4028 (2011).
[47] V.A. Pustovarov, T.V. Perevalov, V.A. Gritsenko, T.P. Smirnova and A.P. Yelisseyev, Thin Solid Films, 519, 6319–6322 (2011).
[48] C. Lin, M. Yu, Z. Cheng, C. Zhang, Q. Meng and J. Lin, Inorg. Chem., 47, 49–55 (2008).
[49] D. Dasgupta, F. Demichelis, C.F. Pirri and A. Tagliaferro, Phys. Rev. B., 43, 2131–2135 (1991).
[50] R. Hari Krishna, B.M. Nagabhushana, H. Nagabhushana, R.P.S. Chakradhar, N. Suriya Murthy, R. Sivaramakrishna, C. Shivakumara, J.L. Rao and T. Thomas, J. Alloys Comp., 589, 596–603 (2014).
[51] R. Hari Krishna, B.M. Nagabhushana, H. Nagabhushana, R.P.S. Chakradhar, R. Sivaramakrishna, C. Shivakumara and T. Thomas, J. Alloys Comp., 585, 129–137 (2014).
[52] S. Wang, C. Zhang, G. Sun, Y. Yuan, L. Chen, X. Xiang, Q. Ding, B. Chen, Z. Li and X. Zu, J. Lumin., 153, 393–400 (2014).
[53] B. Umesha, B. Eraiah, H. Nagabhushana, B.M. Nagabhushana, G. Nagaraja, C. Shivakumara and R.P.S. Chakradhar, J. Alloys Comp., 509, 1146–1151 (2011).
[54] C. Hu, H. Liu, W. Dong, Y. Zhang, G. Bao, C. Lao and Z.L. Wang, Adv. Mater., 19, 470–474 (2007).
[55] Y. Zhang, K. Han, T. Cheng and Z. Fang, Inorg. Chem., 46, 4713–4717 (2007).